

# Pulsed Electrodeposition of Reduced Graphene Oxide on Glass Carbon Electrode as an Effective Support of Electrodeposited Pt Microspherical Particles: Nucleation Studies and the Application for Methanol Electro-Oxidation

Weichun Ye<sup>1,\*</sup>, Xiujun Zhang<sup>1</sup>, Yang Chen<sup>1</sup>, Yongling Du<sup>1</sup>, Feng Zhou<sup>2</sup>, Chunming Wang<sup>1,\*</sup>

<sup>1</sup> Department of Chemistry and Key Laboratory of Nonferrous Metal Chemistry and Resources Utilization of Gansu Province, Lanzhou University, Lanzhou 73000, China

<sup>2</sup> State Key Laboratory of Solid Lubrication, Lanzhou Institute of Chemical Physics, Chinese Academy of Sciences, Lanzhou 730000, China

\*E-mail: [yewch@lzu.edu.cn](mailto:yewch@lzu.edu.cn); [wangcm@lzu.edu.cn](mailto:wangcm@lzu.edu.cn)

Received: 10 December 2012 / Accepted: 11 January 2013 / Published: 1 February 2013

---

Reduced graphene oxide (RGO) film on a glass carbon electrode (GCE) obtained by pulsed electrodeposition has been used as an effective support for the electrodeposition of Pt microspherical particles. The nucleation studies of Pt particles on the RGO film show that the RGO film is advantageous for rapid Pt nucleation and thus results in a rapid growth process of Pt compared to a bare GCE. The electrocatalytic abilities of the Pt catalysts toward methanol oxidation were investigated by cyclic voltammetry, chronoamperometry and Tafel plot, including electrochemical surface area, peak current density, the turnover number and Tafel slope. It is found that the Pt/RGO/GCE electrode has higher catalytic activity and better stability than the Pt/GCE electrode under the same conditions, which indicates that the increased electrocatalytic activity is attributed to the synergistic effect of graphene and Pt particles. The kinetic characterization of Pt/RGO/GCE for methanol electro-oxidation is further discussed.

---

**Keywords:** Pulsed electrodeposition; Graphene; Pt microspherical particle; Nucleation; Methanol electro-oxidation

## 1. INTRODUCTION

Direct methanol fuel cells (DMFCs) have been considered excellent candidates for the next generation of portable power sources because of their advantages such as high energy density and efficiency, low weight, applications to portable systems, fast recharge-time and use of an easy-handling liquid fuel [1,2]. Up to date, platinum based catalysts have been extensively studied;

however, a major problem is the poisoning of catalyst surfaces by carbon monoxide, leading to inhibition and the consequent need to regenerate or replace the catalyst [3-6]. To deal with this problem, the development of new CO-tolerant electrocatalysts for methanol oxidation is principally based on carbon-support design such as black carbon, nanofibers, mesoporous carbon [7]. Yet, the pristine surface of glassy carbon (GC) and carbon nanoparticles are relatively inert and difficult to support Pt particle dispersion homogeneously [8,9], which usually leads to the agglomeration of nanoparticles and affects the catalytic efficiency of Pt particles for methanol electro-oxidation.

Graphene, as a new kind of two-dimensional carbon material with a single (or a few) atomic layer, has been found as a promising candidate for catalyst support in DMFCs due to their unique properties such as the high surface area (theoretical value of 2620 m<sup>2</sup>/g), high conductivity and unique graphitized basal plane structure [10,11]. In particular, graphene-supported Pt-based catalysts are expected to open a novel and insightful way to exploit the applications of DMFCs. For example, platinum–ruthenium nanoparticles were dispersed on graphene nanosheets by a hydrothermal method [12]. Our group [13,14] has reported a chemical reduction method to synthesize Pt/graphene composites and PtPdAu alloys on graphene. However, such preparation techniques have intrinsic drawbacks like involving toxic chemical and the incompatibility of the thermal reduction process [15].

Recently, electrodeposition is arising an effective and controllable alternative technique to synthesize metal nanoparticles supported on graphene for the promising applications of electrocatalysis [16-18] and sensors [19,20]. The technique is surfactant-free and cost-effective and allows to tune the size and composition of particles by changing electrolyte composition and applied potential. The size, distribution and morphology of metal particles are extremely dependent on the nucleation mode, where the size and morphology have a particularly remarkable effect on the intrinsic properties of particles. Therefore, it becomes necessary to study in detail the nucleation mode of metal electrodeposition on graphene, which is important in the fundamental research.

Moreover, electrochemical method is also one promising green strategy for graphene synthesis, especially when Luo group [21] has reported one-step electrochemical process to directly deposit reduced graphene oxide (RGO) film on electrodes from graphene oxide (GO) dispersions by means of cyclic voltammetry (CV). Nonetheless, CV is one of potential cycling methods; its potentials are controlled at different scanning rate over time with a triangle waveform. Pulsed electrodeposition through a potentiostatic or galvanostatic technique is easier to control the size and composition of the deposits simply by varying experimental parameters such as on/off time and peak current density or peak potential [22].

In this work, we firstly develop one-step synthesis route of RGO films on glass carbon electrode (GCE) by using pulsed electrodeposition, which is based on the work of Luo group [21]. The synthesized RGO film is characterized with Raman spectroscopy and X-ray photoelectron spectroscopy (XPS) analysis. The electrode interfaces of the RGO film are characterized with [Fe(CN)<sub>6</sub><sup>3-/4-</sup>] as the electrochemical probe. Then, Pt particles with microspherical structures have been electrodeposited on RGO by using constant potential electrolysis at  $E = -0.25$  V. The nucleation mode of the Pt particles on RGO is investigated with CV, chronocoulometry, chronoamperometry and SEM, as compared with the deposition behaviors of Pt particles on bare GCE. Finally, the catalytic activity and stability of the Pt/RGO/GCE electrode (forming from Pt particles electrodeposited on RGO/GCE

electrode) for the oxidation of methanol are evaluated by using CV, chronoamperometry and Tafel plot. And its kinetic characterization is further studied.

## 2. EXPERIMENTAL

### 2.1 Electrodeposition of RGO film

GO was synthesized from natural expandable graphite by the Hummers method. The as-prepared GO colloid solution was diluted to a concentration of  $1.0 \text{ mg ml}^{-1}$  with  $0.067 \text{ M}$  pH 9.18 phosphate buffer solution (PBS) and then used for the following electrodeposition process.

Prior to electrodeposition, GCE was in turn polished with  $0.3$  and  $0.05 \text{ }\mu\text{M}$  alumina powders, and then sequentially sonicated in double-distilled water and anhydrous ethanol. The electrodeposition of RGO was performed under pulsed electrodeposition technique with 1000 cycles in the GO colloid solution under  $\text{N}_2$  bubbling, as shown in Fig. 1A. The obtained RGO film was named as RGO/GCE. For comparison, GO film on GCE was obtained using chronoamperometrical method at  $0.6 \text{ V}$  for  $2000 \text{ s}$  (Fig. 1B); the GO film on GCE was named as GO/GCE.

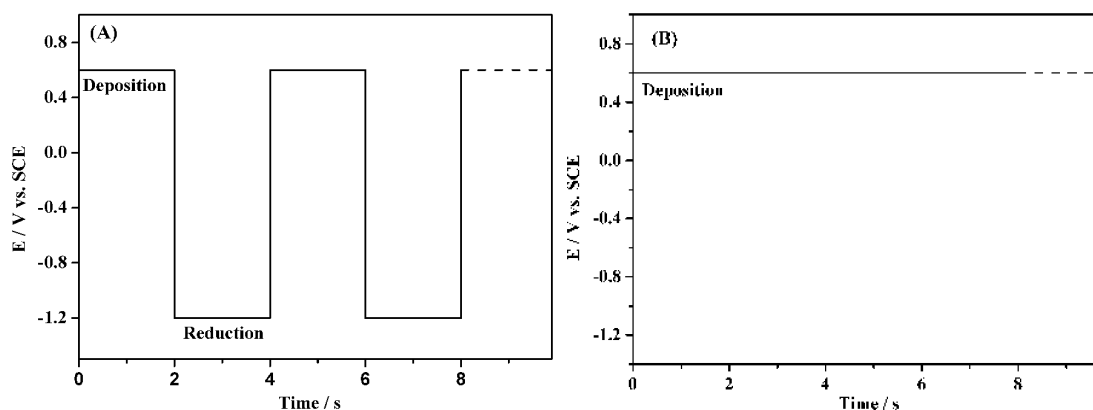


**Figure 1.** (A) Pulsed electrodeposition mode for the deposition of RGO on GCE. (B) Constant potential mode for the deposition of GO on GCE.

The electrochemical experiments were carried out on a CHI 660B electrochemical station (Shanghai China) with a three-electrode system, in which the Pt foil and saturated calomel electrode (SCE) acted as the counter and reference electrodes, respectively. The electrode interfaces of RGO/GCE and GO/GCE were characterized with CV and electrochemical impedance spectroscopy (EIS) in the probing electrolyte of  $5.0 \text{ mM K}_4\text{Fe(CN)}_6/\text{K}_3\text{Fe(CN)}_6$  and  $0.1 \text{ M KCl}$ .

### 2.2 Electrochemical deposition of Pt particles on RGO/GCE

The electrochemical deposition of Pt particles on RGO/GCE or bare GCE was performed in the plating electrolyte of  $3 \text{ mM H}_2\text{PtCl}_6$  and  $0.5 \text{ M H}_2\text{SO}_4$  using constant potential electrolysis at  $E = -0.25$

V for 600 s, naming as Pt/RGO/GCE. For comparison, Pt particles were deposited on bare GCE in the same manner, naming as Pt/GCE.

CV, chronocoulometry and chronoamperometry were used to analyze electrochemical platinum deposition. In CV, the potential was scanned from 1.2 to  $-0.2$  V at  $20 \text{ mV s}^{-1}$ . About chronocoulometry parameters, the potential was from 0.5 to 0 V and pulse width was 10 s. Current-time transient for Pt electrodeposition was recorded at  $E = -0.25$  V. The solution was also the mixture of 3 mM  $\text{H}_2\text{PtCl}_6$  and 0.5 M  $\text{H}_2\text{SO}_4$ .

### 2.3 Methanol electro-oxidation

The electrocatalytic activity and stability of the Pt/RGO/GCE (600 s Pt deposition) for the oxidation of methanol were evaluated in 2 M  $\text{CH}_3\text{OH}$  and 0.5 M  $\text{H}_2\text{SO}_4$  by means of CV, chronoamperometry and Tafel plot. And the catalytic activity of Pt/GCE (600 s Pt deposition) toward methanol electro-oxidation was evaluated under the same conditions.

### 2.4 Characterization

The morphologies of the samples were characterized with a field emission scanning electron microscope (FE-SEM, JSM-6701F, JEOL Inc., Japan). Transmission electron microscopy (TEM, JEM-1230) operating at 200 kV was applied to characterize the morphology of GO. The composition of the samples was tested by XPS (PHI-5702, Physical Electronics, USA; monochromated Al-K $\alpha$  irradiation, with the binding energy of Au4f at 84.8 eV as reference). Raman spectroscopy (Renishaw Microscope, Lab RAMHR800; laser excitation at 532 nm) was used to characterize the obtained RGO film and GO film.

## 3. RESULTS AND DISCUSSION

### 3.1 Pulsed electrodeposition of RGO film on GCE

GO colloids exhibit negative charges through negative electrostatic repulsion originating from ionization of carboxylic acid and phenolic hydroxyl groups on the GO sheets, thus resulting in a good dispersion in water [23]. So, as applying a positive potential, GO sheets could be deposited on the electrode. According to the previous work [21], the as-deposited GO sheets can be electrochemically reduced at  $E = -1.1$  V/SCE. Herein, we use pulsed potential deposition method to achieve the electrodeposition of RGO films because pulsed potential deposition is a higher efficiency compared to CV, in which 0.6 V/SCE is used to deposit GO sheets on GCE, followed by applying  $-1.2$  V/SCE to electrochemically reduce the as-deposited GO sheets to RGO sheets (Fig. 1A). To obtain the GO film, constant potential electrolysis (positive potential) mode is used (Fig. 1B).

TEM, SEM, Raman and XPS techniques were used to characterize the as-prepared GO/GCE and RGO/GCE film. Fig. 2A reveals that the graphite oxide was entirely exfoliated as individual GO

sheets with transparent and ripple-like paper morphology. The surface morphology of the RGO film obtained by pulsed electrodeposition was characterized by SEM. As shown in Fig. 2B, the surface of the film exhibits a wrinkled texture associating with the presence of flexible and ultrathin graphene sheets. Raman spectroscopy is a conventional and powerful technique for the identification and characterization of graphene layers [24-27]. Fig. 2C gives the Raman spectra of GO/GCE and RGO/GCE. The D band and G band located at 1352 and 1585  $\text{cm}^{-1}$  (respectively) in the Raman spectrum of GO/GCE. Similarly, RGO/GCE also contained D band and G band (at 1352 and 1590  $\text{cm}^{-1}$ , respectively), which is in good agreement with the report of Ferrari et al. [26]. The intensity ratio of the D to G band ( $I_D/I_G$ ) is generally accepted that the  $I_D/I_G$  reflects the defect density of carbonaceous materials. For RGO/GCE, the  $I_D/I_G$  value was calculated as 1.55, while the value decreased to 1.02 for GO/GCE. The increased  $I_D/I_G$  value may be attributed to the lower defect concentration in RGO than in GO [27].

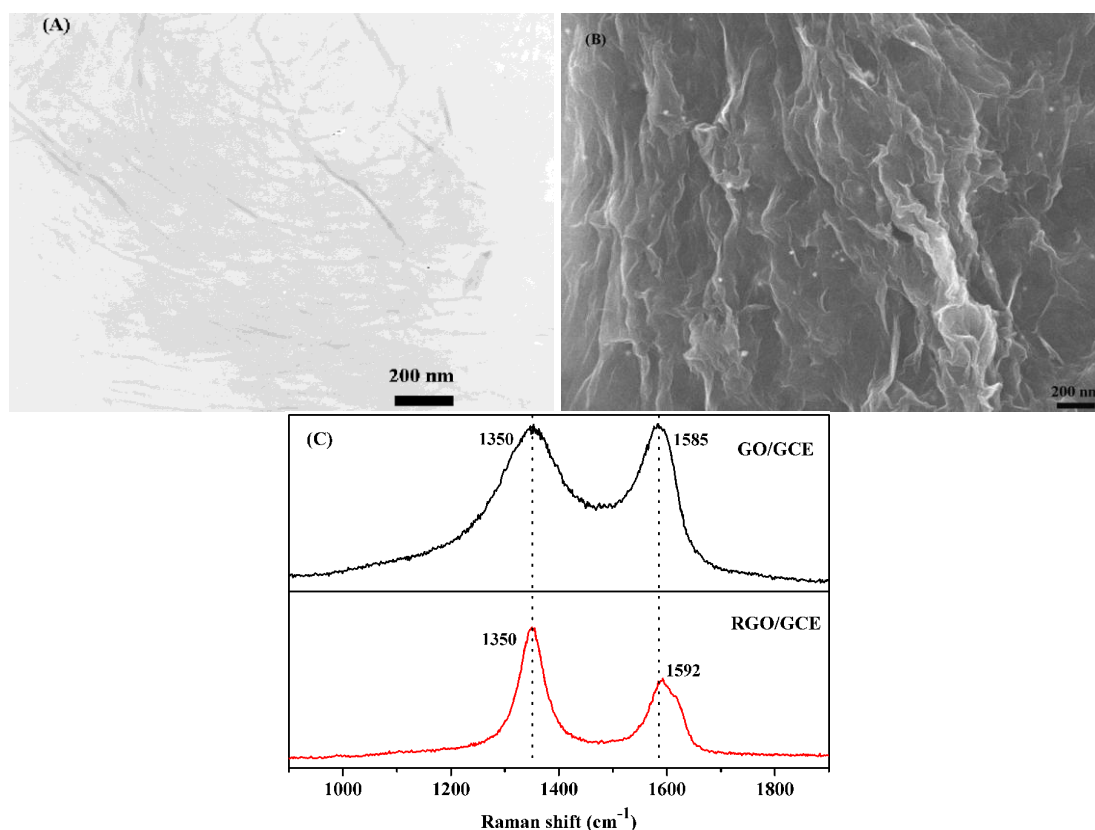


**Figure 2.** (A) TEM image of GO colloid and (B) SEM image of RGO electrodeposited on GCE. (C) Raman spectra of GO/GCE and RGO/GCE.

The XPS spectrum can be used to observe the inner structure of C for carbon-based materials. The high-resolution of C1s XPS spectra for GO and RGO are shown in Figs. 3A and 3B, which presents different functional groups corresponding to carbon atoms: C-C/C=C ( $\text{sp}^2/\text{sp}^3$  hybridized carbon atoms in aromatic rings, 284.7 eV), C-O (286.8 eV) and C=O (carbonyl, 288.2 eV) [28]. The spectrum of RGO shows a significant reduction of oxygen-containing groups compared to the GO,

indicating graphene has been converted from GO by removing the surface functional groups via electrochemical reduction.

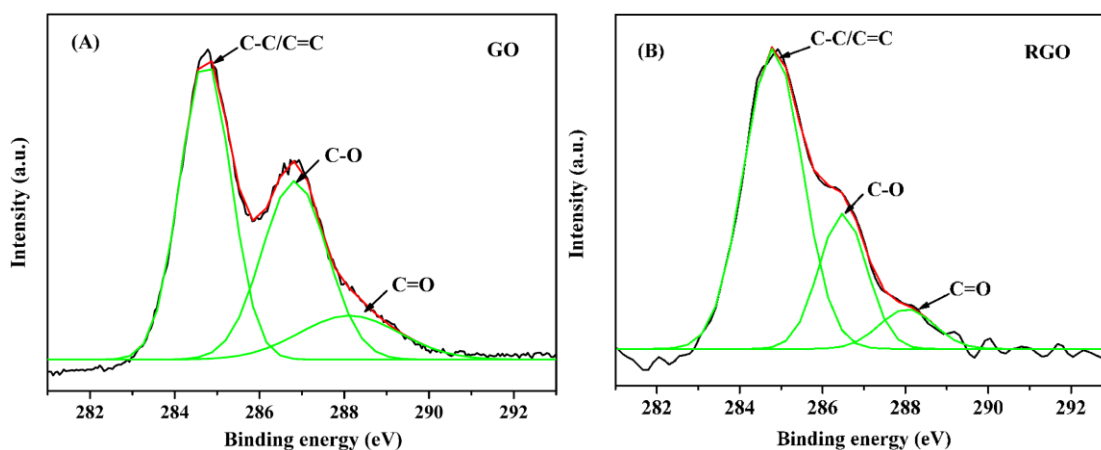


**Figure 3.** C1s XPS spectra of GO (A) and RGO (B) films electrodeposited on GCE.

Furthermore, the electrochemical properties of GO/GCE, RGO/GCE and bare GCE were tested by CV and EIS exploiting the solution-based redox probe  $[\text{Fe}(\text{CN})_6]^{3-/4-}$ , as shown in Fig. 4. And the corresponding parameters are displayed in Table 1, including peak potential difference ( $\Delta E_p$ ), oxidation peak current ( $I_p^{\text{Ox}}$ ) and charge transfer resistance ( $R_{ct}$ ). In the CV (Fig. 4A), sigmoidal cyclic voltammetric curves with a pair of redox peaks were obtained. When GO was deposited onto the GCE surface (curve a), the  $\Delta E_p$  value dramatically increased (560 vs. 277 mV) while the  $I_p^{\text{Ox}}$  decreased ( $0.92$  vs.  $0.94 \text{ mA cm}^{-2}$ ) as compared with the bare GCE (curve c).  $\Delta E_p$  is inversely proportional to the electron transfer rate, so the results suggest that the GO film acts as an insulating layer, resulting in the interfacial electron transfer difficult due to their disrupted  $sp^2$  bonding networks.

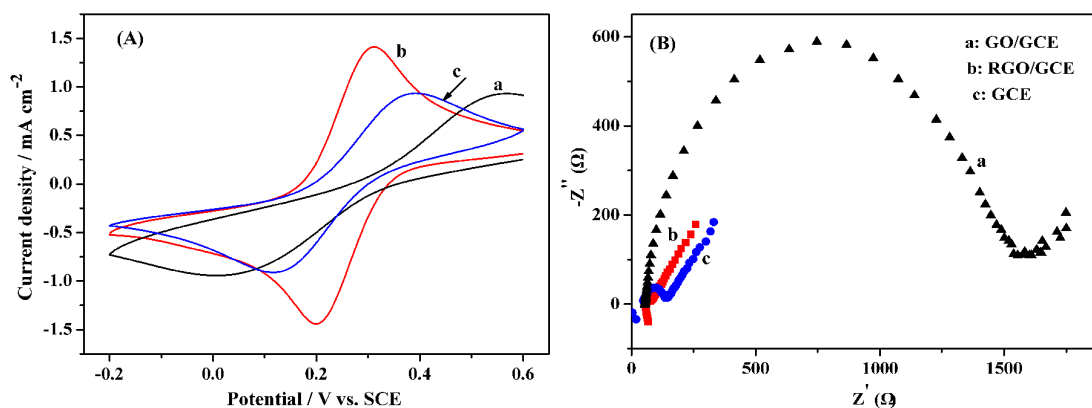


**Figure 4.** Cyclic voltammograms (A) and electrochemical impedance spectroscopy (EIS) (B) of GO/GCE (curve a), RGO/GCE (curve b) and GCE (curve c) in the probing electrolyte of 5.0 mM  $\text{K}_4\text{Fe}(\text{CN})_6/\text{K}_3\text{Fe}(\text{CN})_6$  and 0.1 M KCl. In CV, scan rate was  $50 \text{ mV s}^{-1}$ .

Contrarily, at the RGO modified GCE (curve b), the  $\Delta E_p$  value was reduced to 109 mV, implying that RGO accelerated electron transfer between the probe and the electrode, which is attributed to the fact that RGO has a graphitic network of  $sp^2$  bonds and thus the electrical conductivity of the RGO sheets is significantly improved [29]. These results were further confirmed by the EIS measurements. In the EIS (Fig. 4B), the semicircle portion observed at high frequencies corresponds to the electron transfer limiting process. The  $R_{ct}$  value dramatically increased for GO modified on GCE (curve a), while the value decreased distinctively for RGO deposited on GCE (curve b), compared with bare GCE (curve c).

**Table 1.** The electrochemical parameters from Fig. 4.

	$\Delta E_p$ , mV	$I_p^{Ox}$ , mA cm <sup>-2</sup>	$R_{ct}$ , $\Omega$
GCE	277	0.94	90
GO/GCE	560	0.92	1502
RGCO/GCE	109	1.42	24

### 3.2 Electrochemical studies of Pt electrodeposition on RGO/GCE

The comparison of platinum electrochemical growth process on between RGO/GCE and bare GCE was investigated by CV, chronocoulometry and chronoamperometry. Fig. 5 illustrates the first cyclic voltammograms for a solution of 3 mM  $H_2PtCl_6$  and 0.5 M  $H_2SO_4$  at RGO/GCE and bare GCE. The first scan contains a characteristic “nucleation loop”, which arises from the greater overpotential required for nucleation onto the electrode compared to deposition of metal onto metal [30]. Regardless of the RGO/GCE electrode or bare GCE electrode, a reduction peak of Pt and the oxidation peak of deposited Pt can be seen and the peak at  $-0.14$  V is related to the reduction of hydrogen ions to hydrogen adatoms [31].

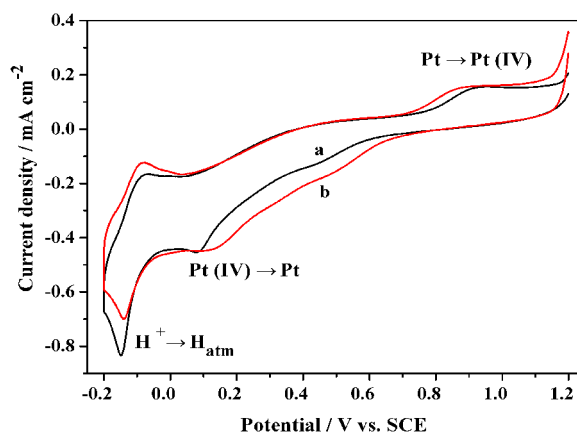


**Figure 5.** Cyclic voltammograms for Pt electrodeposition on GCE (a) and RGO/GCE (b) in 0.5 M  $H_2SO_4$  solution containing 3 mM  $H_2PtCl_6$  at a scan rate of 20 mV s<sup>-1</sup>.

However, it is found that the rate of heterogeneous electron transfer to the  $[\text{PtCl}_6]^{2-}$  ions in solution is affected by the presence of RGO. The platinum reduction peak potential shifts in a positive potential direction about 40 mV, indicating that nucleation on the RGO/GCE electrode is thermodynamically easier than on the bare GCE interface.

Chronocoulometry is another electrochemical technique to evaluate the electrodeposition behaviors [32]. Fig. 6A shows the chronocoulograms of Pt electrodeposition on GCE (a) and RGO/GCE (b) in 0.5 M  $\text{H}_2\text{SO}_4$  solution containing 3 mM  $\text{H}_2\text{PtCl}_6$ , and the corresponding  $Q$  versus  $t^{1/2}$  plots are displayed in Fig. 6B. The diffusion coefficient  $D$  can be measured according to Cottrell equation [33]:

$$Q = 2nFAc_0D^{1/2}\pi^{1/2}t^{1/2} \quad (1)$$

Here,  $c_0 = 3$  mM,  $A = 0.196$  cm<sup>2</sup> and  $n = 4$ . The slope of the plots is used to calculate the  $Q/t^{1/2}$  value. The calculated diffusion coefficient ( $D$ ) for Pt electrodeposition at the RGO/GCE electrode is as high as 1.9 times that at bare GCE electrode ( $5.9 \times 10^{-5}$  vs.  $3.1 \times 10^{-5}$  cm<sup>2</sup> s<sup>-1</sup>). These results suggest that nucleation on the RGO/GCE surface is thermodynamically favored compared with that on the bare ITO surface and most likely reflect a reduction in the activation energy of surface diffusion of adions ( $E_{\text{adi}}$ ) at the modified surface.

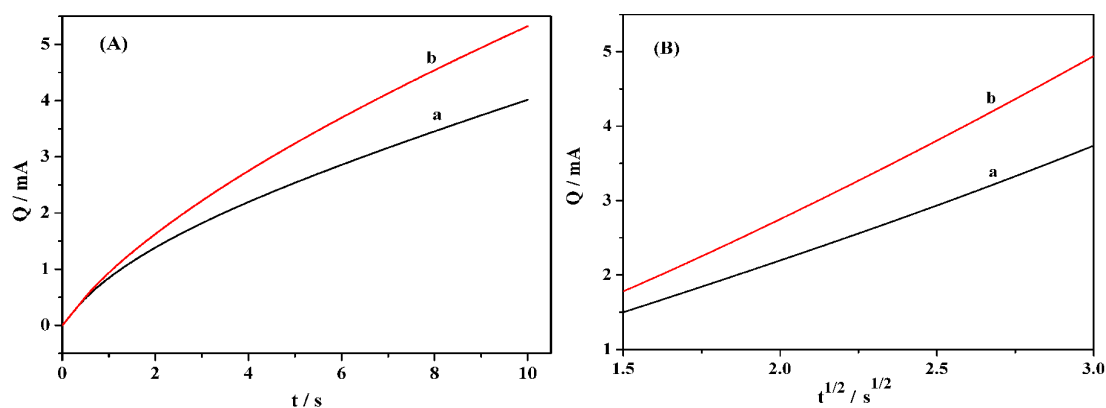


**Figure 6.** (A) Chronocoulograms of Pt electrodeposition on GCE (a) and RGO/GCE (b) in 0.5 M  $\text{H}_2\text{SO}_4$  solution containing 3 mM  $\text{H}_2\text{PtCl}_6$ . (B) Plots of  $Q$  versus  $t^{1/2}$ .

The applied electrodeposition potential of Pt (-0.25 V/SCE) is more negative than the platinum reduction peak potential ( $\sim 0.1$  V). Therefore, 2-dimensional (2D) deposition of Pt onto the substrates of RGO/GCE or GCE can be ruled out and the high overpotential results in a shift from progressive 3D diffusion limited nucleation and growth to instantaneous 3D diffusion limited nucleation and growth [34,35]. The non-dimensional plots of  $(i/i_{\text{max}})^2$  vs.  $t/t_{\text{max}}$  are widely used for the determination of the nucleation and growth type by comparing theoretical values and experimental results.  $i_{\text{max}}$  and  $t_{\text{max}}$  represent the maximum peak current of the recorded  $i-t$  transient and the corresponding time, respectively. Fig. 7 shows the  $[(i/i_{\text{max}})^2$  vs.  $t/t_{\text{max}}$ ] plots for electrodeposition from 3 mM  $\text{H}_2\text{PtCl}_6$  solution in 0.5 M  $\text{H}_2\text{SO}_4$  to GCE (curve a):  $i_{\text{max}} = 1.56$  mA cm<sup>-2</sup>,  $t_{\text{max}} = 1.3$  s; and RGO/GCE (curve b):

$i_{\max} = 2.94 \text{ mA cm}^{-2}$ ,  $t_{\max} = 0.4 \text{ s}$ . Equations. 2 and 3 express the cases of instantaneous and progressive nucleation as proposed by Sharifker and Hills [36]:

$$\left(\frac{i}{i_{\max}}\right)^2 = 1.9542 \frac{t_{\max}}{t} \left\{1 - \exp\left(-1.2564 \frac{t}{t_{\max}}\right)\right\}^2 \quad (2)$$

$$\left(\frac{i}{i_{\max}}\right)^2 = 1.2254 \frac{t_{\max}}{t} \left\{1 - \exp\left[-2.3367\left(\frac{t}{t_{\max}}\right)^2\right]\right\}^2 \quad (3)$$

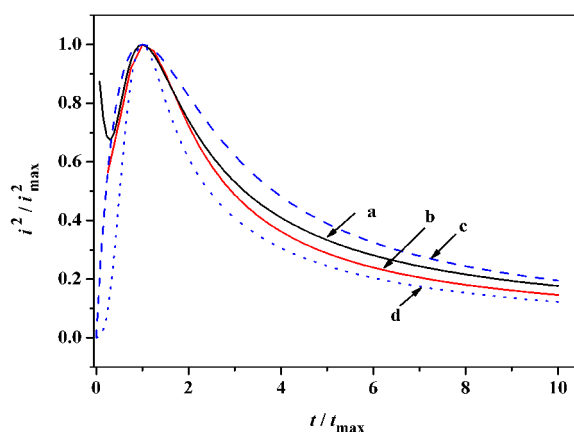


**Figure 7.**  $(i^2 / i_{\max}^2)$  vs.  $(t / t_{\max})$  plots for chronoamperometric deposition of Pt particles from 3 mM  $\text{H}_2\text{PtCl}_6$  in 0.5 M  $\text{H}_2\text{SO}_4$  at  $E = -0.25 \text{ V/SCE}$  on GCE (a) and RGO/GCE (b); theoretical curves for instantaneous (dashed line, curve c) and progressive nucleation (dotted line, curve d).

It is clearly seen from Fig. 7 that both electrochemical reduction processes of Pt(IV) on the bare GCE and RGO/GCE electrodes undergo between an instantaneous nucleation process and a progressive nucleation process. Nonetheless, the electrodeposition process of Pt on RGO/GCE is more close to the progressive nucleation process, while the case for Pt deposition on bare GCE is inverse, *i.e.*, it is relatively close to the instantaneous nucleation process. For instantaneous nucleation, the nuclei number rapidly reaches a value that is constant. In the case of progressive nucleation, new nuclei are formed continuously. Therefore, this indicates that the RGO film is advantageous for rapid Pt nucleation and results in rapid growth process of Pt.

As discussed above from the measurements of CV, chronocoulometry and chronoamperometry, the addition the RGO film is favorable to accelerate the formation of Pt nuclei. This may be attributed to the two reasons: one is that graphene sheet has a large specific surface area and exhibits a unique of 2D structure, which is advantageous to deposition of Pt particles [37]; the other is that the RGO/GCE has a relatively more rapid charge transfer rate and a lower charge transfer resistance  $R_{ct}$ , being 24 vs. 90  $\Omega$  for RGO/GCE and GCE, respectively, so the GCE electrode is kinetically rather sluggish.

### 3.3 SEM characterization of Pt particles

Fig. 8 shows the SEM images of Pt particles electrodeposited on bare GCE (A and B) and RGO/GCE (C and D) for 600 s under constant potential electrolysis at  $-0.25$  V/SCE. It is clearly observed that the RGO film affects the morphology and size of the electrodeposited Pt particles. On the RGO film, the Pt particles integrate uniformly on the RGO surface, and they exhibit a spherical shape with a diameter of ca.  $1.2$   $\mu\text{m}$ . Each microsphere is built up by numerous small Pt nanorods with average diameter of  $\sim 30$  nm and the length of  $\sim 90$  nm (Fig. 8D). However, as Pt particles were electrodeposited on the bare GCE under the same conditions, Pt particles are formed as flowerlike particles, which are built up with numerous small Pt nanoparticles, and these small nanoparticles are interconnected with one another to form larger architectures (Fig. 8B). Also, the diameter of the flowerlike particles on GCE is only about  $150\sim 300$  nm.

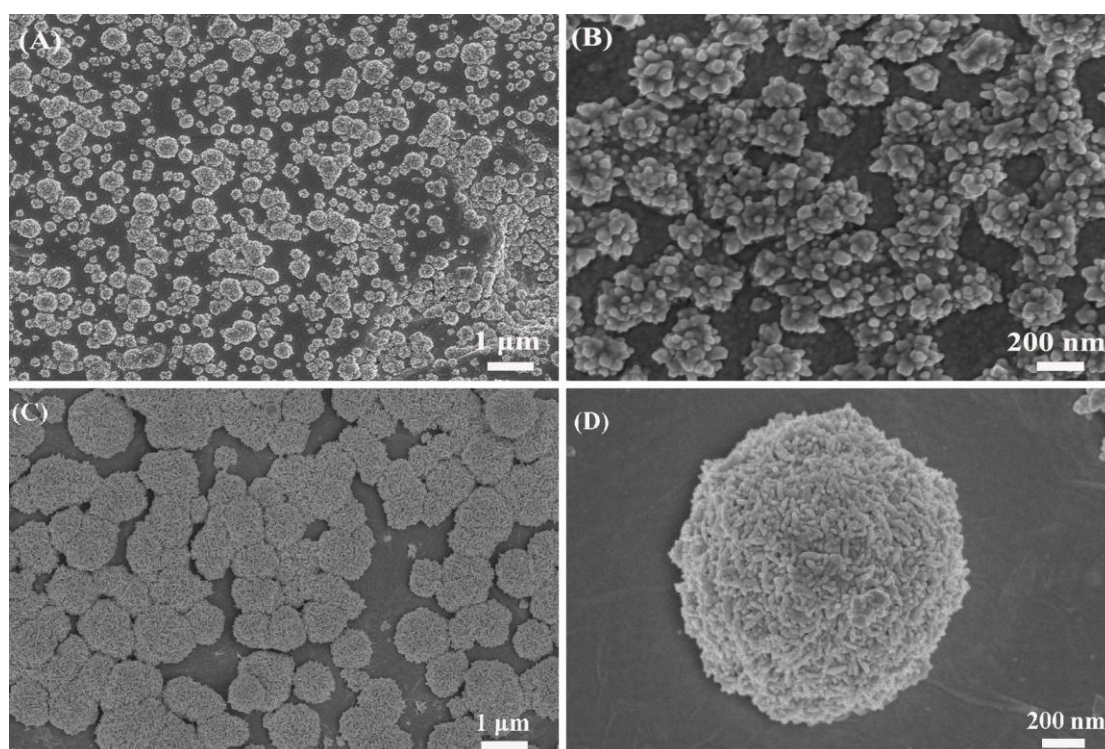


**Figure 8.** SEM images of the Pt particles electrodeposited on bare GCE surface (A and B) and on the surface of RGO/GCE (C, D) under the constant potential of  $-0.25$  V for 600 s in  $0.5$  M  $\text{H}_2\text{SO}_4$  solution containing  $3$  mM  $\text{H}_2\text{PtCl}_6$ .

As we know, the electrodeposition process involves two processes: diffusion process, the mass transfer of metal ions from the bulk solution through the diffusive layer towards the electrode surface, and activation process, the reduction reaction on the electrode [38]. According to our previous analysis for electroless deposition of Pt particles with microspherical and flowerlike structures on silicon [39], the shape control of the crystals can be achieved by manipulating the growth kinetics. From the electrochemical results, the diffusion coefficient ( $D$ ) for Pt electrodeposition at the RGO/GCE

electrode is larger than that at bare GCE electrode, which promotes the burst of initial homogeneous nucleation. Therefore, these Pt nuclei aggregate fast together and finally form microspherical structures. By contrast, the speed of Pt homogeneous nucleation on bare GCE is much slower; only a few nuclei can aggregate together, so the formed Pt particles exhibit a flowerlike structure and have a smaller diameter.

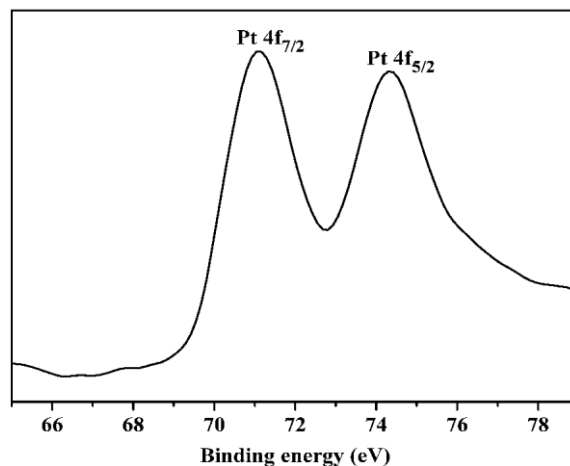


**Figure 9.** Pt4f XPS spectrum of Pt/RGO/GCE.

To further verify the Pt composition of the microspheres, an XPS experiment was performed, and the result is shown in Fig. 9. We can observe that two XPS bands located at 71.1 and 74.4 eV, corresponding to the Pt 4f<sub>7/2</sub> and Pt 4f<sub>5/2</sub> signal, respectively, which demonstrates the formation of Pt(0) state.

### 3.4 Comparison of Methanol electro-oxidation at Pt/RGO/GCE and Pt/GCE

The electrochemically active surface area ( $S_{\text{El}}$ ) provides important information regarding the number of electrochemically active sites per gram of the catalyst, and also is a key parameter to compare different electrocatalytic supports. Fig. 10A shows the cyclic voltammograms for Pt/GCE (curve a) and Pt/RGO/GCE (curve b) in 0.5 M H<sub>2</sub>SO<sub>4</sub> solution. As expected for Pt catalysts, the typical hydrogen adsorption/desorption peaks as well as the monolayer oxide (PtOx) reduction peaks in the cathodic sweep are observed. The currents in the adsorption–desorption region for the electrocatalysts are in the sequence of Pt/RGO/GCE > Pt/GCE. The  $S_{\text{El}}$  values are determined by the charge concerning H<sup>+</sup> adsorption,  $Q_{\text{H}}$ , according to the following equation [40]:

$$S_{\text{El}} = \frac{Q_{\text{H}}}{Q_{\text{ref}} \times \text{Pt loading}} \quad (4)$$

According to our calculation, Pt/RGO/GCE has much higher  $S_{EI}$  value ( $43.95 \text{ m}^2 \text{ g}^{-1}$ ) than Pt/GCE ( $11.76 \text{ m}^2 \text{ g}^{-1}$ ).

The electrocatalytic activity of Pt/RGO/GCE for methanol oxidation was evaluated by cyclic voltammetry in 2 M  $\text{CH}_3\text{OH}$  and 0.5 M  $\text{H}_2\text{SO}_4$  electrolyte, and the Pt/GCE composite electrode was also tested under the same conditions for comparison. As shown in Fig. 10B, both CV curves show a similar methanol oxidation current peak in the forward scan and an oxidation peak in the backward scan corresponding to the removal of the residual carbonaceous species formed in the forward scan. Herein, from qualitative analysis to compare the Pt/GCE electrode, three aspects are evident. The data are listed in Table 2. First, a larger enhancement in peak current density is observed at the Pt/RGO/GCE electrode. The forward peak current density ( $I_f$ ) is  $20.44 \text{ mA cm}^{-2}$  for the Pt/RGO/GCE, which is 2.67 times as large as that for Pt/GCE ( $7.65 \text{ mA cm}^{-2}$ ). Similarly, the backward peak current density ( $I_b$ ) of Pt/RGO/GCE at the onset potential is also about 2.6 times as large as that of Pt/GCE ( $15.41$  versus  $5.92 \text{ mA cm}^{-2}$ ). Second, the peak potential for methanol oxidation at the RGO/GCE electrode shifts to a little more negative value (about 10 mV). Third, the ratio of the forward anodic peak current ( $I_f$ ) to the backward anodic peak current ( $I_b$ ) can be used to evaluate the catalyst tolerance to the intermediate carbonaceous species accumulated on electrode surface [41].

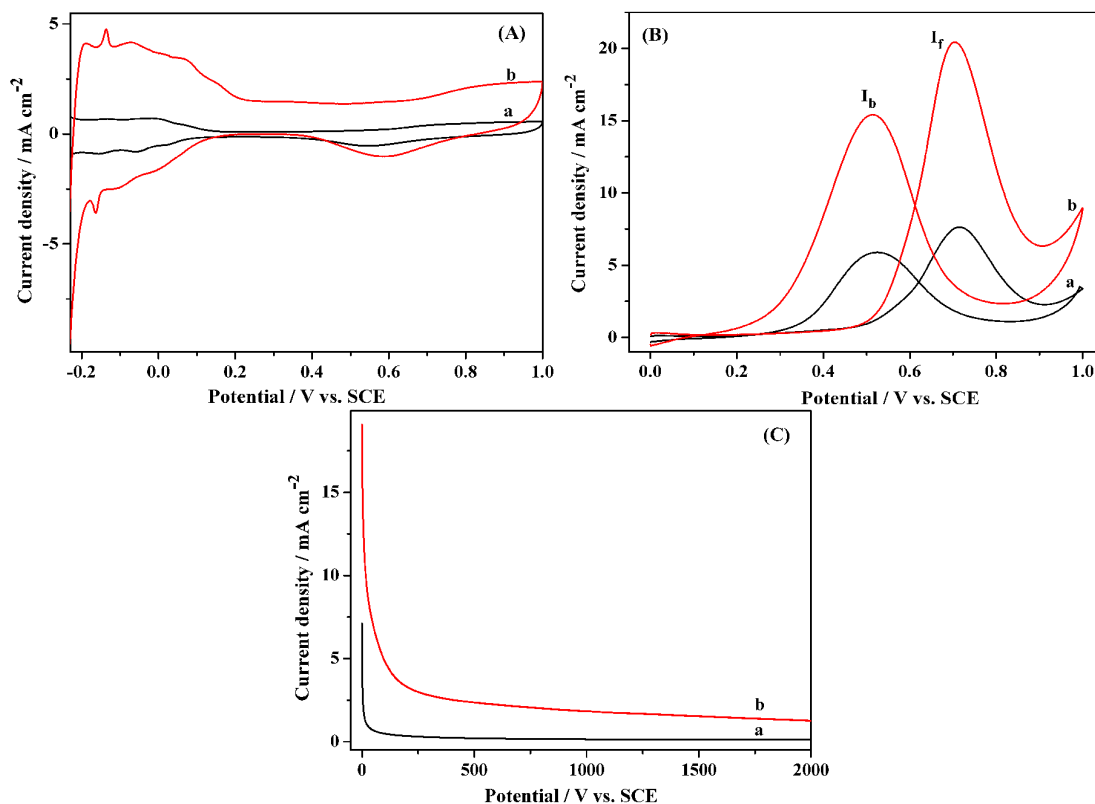


**Figure 10.** Cyclic voltammograms in 0.5 M  $\text{H}_2\text{SO}_4$  solution in the absence (A) or presence (B) of 2 M  $\text{CH}_3\text{OH}$  with the scan rate of  $50 \text{ mV s}^{-1}$ . (C) shows the chronoamperograms at 0.70 V for methanol electro-oxidation of 2 M  $\text{CH}_3\text{OH}$  in 0.5 M  $\text{H}_2\text{SO}_4$ . Curves a and b represent the electrodes of Pt/GCE and Pt/RGO/GCE, respectively.

The higher  $I_f/I_b$  value indicates higher tolerance to intermediate carbon species, which means that methanol can be oxidized to carbon dioxide much more efficiently [42,43]. In this work, the ratios of  $I_f/I_b$  are calculated as 1.33 and 1.29 for Pt/RGO/GCE and Pt/GCE electrodes, respectively. Obviously, Pt/RGO/GCE has less carbonaceous accumulation and thus is much more tolerant toward CO poisoning.

Methanol electro-oxidation at Pt catalysts forms CO and other intermediate carbonaceous species, which hinder further oxidation of methanol and cause the surface poison of Pt catalysts. Hence, the anti-poisoning properties need to be further proved by chronoamperometry. Fig. 10C shows the corresponding  $i-t$  curves for methanol oxidation at 0.70 V. It is noticeable that the current decays associated with the poisoning of the intermediate species followed in the order of Pt/RGO/GCE > Pt/GCE. Pt/RGO/GCE presents a current density of 1.27 mA cm<sup>-2</sup> after 2000 s whereas Pt/GCE only has a current density of 0.12 mA cm<sup>-2</sup>.

To further compare the electrocatalytic efficiency and stability for methanol oxidation at between Pt/RGO/GCE and Pt/GCE, the turnover number (TON) is introduced. The TON is defined as the number of methanol molecules that react per catalyst surface site, which directly reflects the steady-state current density for methanol oxidation. After 2000 s electrocatalysis (Fig. 10C), the current density was considered to be the steady-state current density. For the steady-state current density, the TON is calculated using the following equation:

$$\text{TON} \left( \frac{\text{molecules}}{\text{site}} \right) = \frac{i \times 6.02 \times 10^{23}}{nF \times 1.3 \times 10^{15}} \quad (5)$$

where  $i$  is the steady-state current density after 2000 s scanning,  $n$  is the number of electrons produced by oxidation of 1 mol methanol ( $n = 6$ ),  $F$  is the Faraday constant, and the density of the topmost atoms of an ideal Pt (100) surface is about  $1.3 \times 10^{15}$  cm<sup>-2</sup>. The calculated TONs are to be 1.014 s<sup>-1</sup> and 0.093 s<sup>-1</sup> for the electrodes of Pt/RGO/GCE and Pt/GCE, respectively (Table 2). This implies that the Pt/RGO/GCE electrode is available to electro-catalyze the oxidation of more methanols for the same time with the same number of sites than the Pt/GCE electrode.

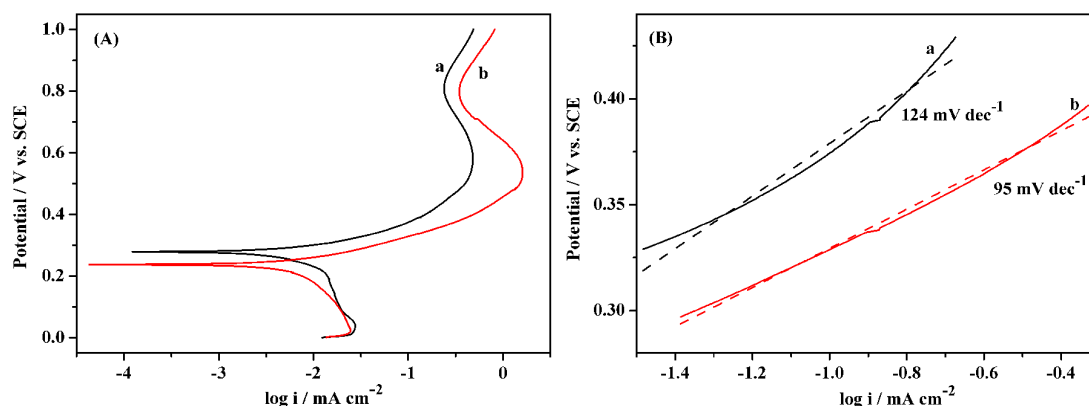


**Figure 11.** Tafel plots (A) and the extracted anode polarization curves (B) of Pt/GCE (curve a) and Pt/RGO/GCE (curve b) in 0.5 M H<sub>2</sub>SO<sub>4</sub> + 2 M CH<sub>3</sub>OH solution. Scan rate: 0.5 mV s<sup>-1</sup>. In (b), the dashed lines were the linear fitting lines.

Various studies on methanol electro-oxidation have shown that the kinetic parameters like Tafel slope, exchange current ( $j_0$ ) and equilibrium potential ( $E_0$ ) are possibly determined by Tafel plots [14]. Fig. 11A compares the Tafel plots of the electrodes of Pt/RGO/GCE and Pt/GCE in 0.5 M H<sub>2</sub>SO<sub>4</sub> + 2 M CH<sub>3</sub>OH aqueous solution. The Tafel plots were recorded from 0 to 1.0 V with a scan rate of 0.5 mV s<sup>-1</sup> and the Tafel parameters are listed in Table 2. According to the Butler-Volmer expression for an oxidation process [33]:

$$\eta = -\frac{2.303RT}{\beta nF} \log j_0 + \frac{2.303RT}{\beta nF} \log j \quad (6)$$

where  $j$  is the electrode current;  $j_0$  is the exchange current which is calculated according to the Tafel extrapolation method;  $n$  is number of electrons involved in the electrode reaction;  $\beta$  is the anodic transfer coefficient;  $\eta$  is overpotential and  $\frac{2.303RT}{\beta nF}$  is Tafel slope. Tafel plot is derived from the polarization curves to obtain the Tafel slope. Fig. 11B gives the extracted anode polarization curves from Fig. 11A, the potentials being from 0.3 to 0.45 V. It can be seen in Table 2 that the  $j_0$  and Tafel slope for the Pt/RGO/GCE electrode are smaller than those for the Pt/GCE electrode under the same conditions, and the  $E_0$  value also shifts negatively. According to Equation 5, we can conclude that the lower the values of Tafel slope and  $j_0$ , the smaller  $\eta$  and the higher the reaction activity. Thus, the Pt/RGO/GCE electrode has higher catalytic activity for methanol electro-oxidation, which is well consistent with the above analysis.

These electrochemical results of methanol electro-oxidation imply the dispersed Pt particles and the RGO film might have synergistic electrocatalytic effect on methanol oxidation [18,44]. So, it can be concluded that RGO is more suitable than GCE as a catalytic support.

**Table 2.** Comparison of electrochemical parameters for methanol electro-oxidation at Pt/GCE and Pt/RGO/GCE.

	$Q_H$ (mC cm <sup>-2</sup> )	$S_{EI}$ (m <sup>2</sup> g <sup>-1</sup> )	$E_p$ (V)	$I_f$ (mA cm <sup>-2</sup> )	$I_b$ (mA cm <sup>-2</sup> )	$I_f/I_b$	TON (s <sup>-1</sup> )	$E_0$ (V)	$j_0$ (mA cm <sup>-2</sup> )	Tafel slope (mV dec <sup>-1</sup> )
Pt/GCE	2.47	11.76	0.717	7.65	5.92	1.29	0.093	0.279	$3.23 \times 10^{-6}$	124
Pt/RGO/GCE	9.23	43.95	0.706	20.44	15.41	1.33	1.014	0.237	$1.93 \times 10^{-6}$	95

### 3.5 Kinetic investigation of methanol electro-oxidation at Pt/RGO/GCE electrode

The kinetics of methanol electro-oxidation at the Pt/RGO/GCE electrode was further studied. Fig. 12A shows the CV curves for the oxidation of methanol in the solution of 2 M CH<sub>3</sub>OH and 0.5 M H<sub>2</sub>SO<sub>4</sub> at different scan rate based on the Pt/RGO/GCE electrode. The relationship between the forward peak current density ( $i_p$ ) and square root of scan rate ( $v$ ) is presented in Fig. 12B, and a linear

relationship is observed. It can be inferred that the oxidation of methanol may be controlled by a diffusion process. Additionally, the forward peak potential  $E_P$  increased with the scan rate ( $\nu$ ), another linear relationship between  $E_P$  and  $\log(\nu)$  is obtained as shown in Fig. 12C, which suggests that the oxidation of methanol on the electrode is irreversible electrode process.

For an irreversible charge transfer electrode process, the slope of  $E_P$  vs.  $\log(\nu)$  can be described as the following equation:

$$K = \frac{\partial E_P}{\partial \log(\nu)} = \frac{2.3RT}{2\alpha nF} \quad (7)$$

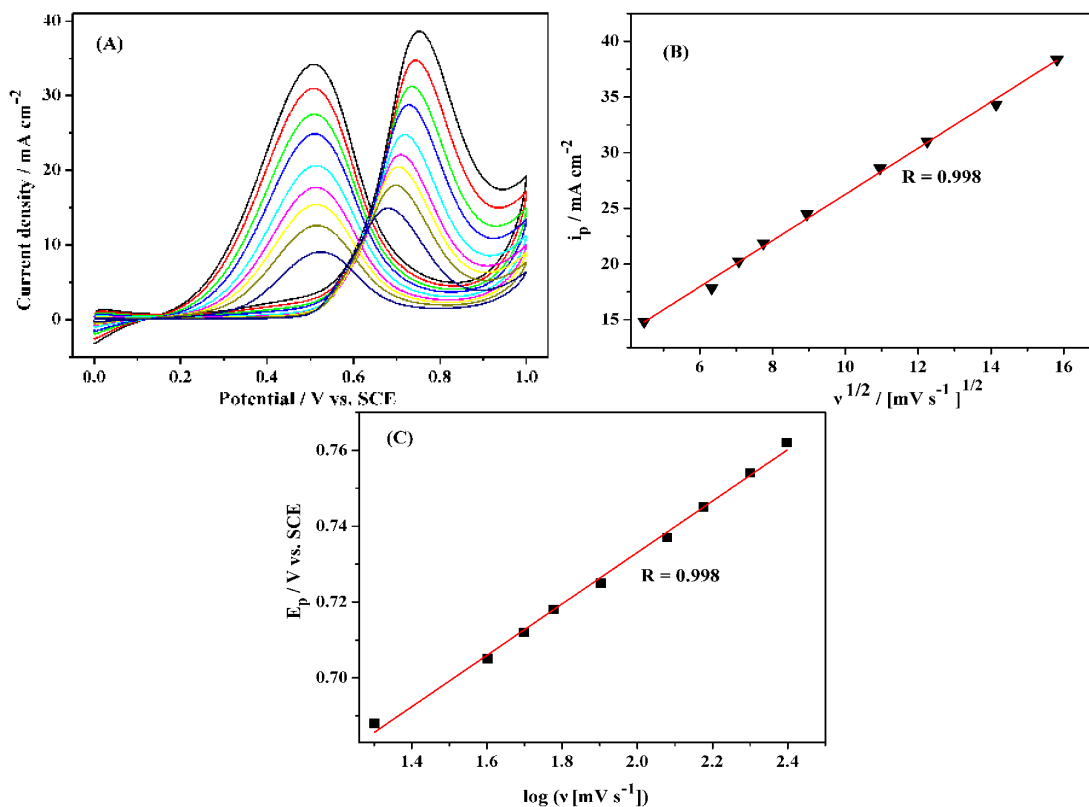


**Figure 12.** (A) CV curves of 2 M CH<sub>3</sub>OH in 0.5 M H<sub>2</sub>SO<sub>4</sub> at Pt/RGO/GCE (Scan rate 20, 40, 50, 60, 80, 120, 150, 200, 250 mV s<sup>-1</sup> from inner to outer). (B)  $i_p$  and  $\nu^{1/2}$  plot and (C)  $E_p$  and  $\log(\nu)$  plot.

Herein,  $\alpha$  stands for the electron transfer coefficient, characterizing the effect of electrochemical potential on the activation energy of an electrochemical reaction. The obtained slope of  $E_P$  vs.  $\log(\nu)$  of is 67.8 mV.  $n\alpha$  is calculated as 0.44. According to the reference [45],  $n$  equals to 1.3. For  $1 < n < 2$ , the chemisorbed poison is essentially linearly and bridge-bonded CO species [46]. Hence,  $\alpha$  can be calculated as 0.34. Additionally, the relationship of between  $i_p$  and  $\nu^{1/2}$  can be written as:

$$i_p = 0.4958 \times 10^{-3} n F^{3/2} (RT)^{-1/2} (\alpha n)^{1/2} A C D^{1/2} v^{1/2} \quad (8)$$

where  $D$  is diffusion coefficient.  $D = 1.5 \times 10^{-8}$  m<sup>2</sup>/s at 293K can be calculated from the plot of  $j_p$  vs.  $v^{1/2}$  for the oxidation peak, which is much higher than the reported values [47,48]. As mentioned above, methanol oxidation is controlled by a diffusion process, thus the higher  $D$  value means a beneficial effect on the kinetics of methanol oxidation.

#### 4. CONCLUSIONS

We have developed one-step electrochemical deposition route on the basis of the work of Luo group, to prepare RGO films on GCE by using pulsed electrodeposition. The RGO film is characterized with SEM, Raman, XPS and the electrochemical analysis. The Pt nucleation studies demonstrate that the RGO film is favorable to electrodeposition of Pt microspherical particles with rapid Pt nucleation compared with bare GCE, which may be attributed that the RGO film has the large specific surface area with a unique of 2D structure and a relatively more rapid charge transfer rate and a lower charge transfer resistance. Meanwhile, the Pt/RGO/GCE electrode exhibits superior electrocatalytic activity and improved stability for methanol oxidation than the Pt/GCE electrode, by means of systematical electrochemical methods. The results are possible due to the synergistic effect of graphene and the Pt microspherical particles. Moreover, the kinetic characterization of Pt/RGO/GCE for methanol electro-oxidation has been also tested. In view of graphene as an effective and promising support material for noble metal loading which have applications in various areas such as electrocatalysis, electroanalysis and sensors, the systematical investigation of the nucleation mechanism of metal electrodeposition on graphene becomes extremely important in the fundamental research involving the nanoparticle size distribution and crystal structure, which affects the application performances of the nanostructured materials.

#### ACKNOWLEDGMENTS

This work is supported by the Natural Science Foundation of Gansu Province, China (No. 1107RJZA261) and the Fundamental Research Funds for the Central Universities (No. lzujbky-2011-25).

#### References

1. R. F. Service, *Science*, 296 (2002) 1222.
2. M. Winter and R. J. Brodd, *Chem. Rev.*, 104 (2004) 4245.
3. Y. Liu, M. Chi, V. Mazumder, K. L. More, S. Soled, J. D. Henao and S. Sun, *Chem. Mater.*, 23 (2011) 4199.
4. L. Dong, R. R. S. Gari, Z. Li, M. M. Craig and S. Hou, *Carbon*, 48 (2010) 781.
5. B. Singh, L. Murad, F. Laffir, C. Dickinson and E. Dempsey, *Nanoscale*, 3 (2011) 3334.
6. W. Ye, H. Kou, Q. Liu, J. Yan, F. Zhou and Wang, C. *Int. J. Hydrog. Energy*, 37 (2012) 4088.

7. E. S. Steigerwalt, G. A. Deluga, D. E. Cliffel and C. M. Lukehart, *J. Phys. Chem. B*, 105 (2001) 8097.
8. S. Zheng, J. Hu, L. Zhong, L. Wan and W. Song, *J. Phys. Chem. C*, 111 (2007) 11174.
9. Y. Yao, Y. Ding, L. Sheng and X. Xia, *Carbon*, 44 (2006) 61.
10. C. Lee, X. Wei, J. W. Kysar and J. Hone, *Science*, 321 (2008) 385.
11. M. D. Stoller, S. Park, Y. Zhu, J. An and R. S. Ruoff, *Nano Lett.*, 8 (2008) 3498.
12. S. H. Lee, N. Kakati, S. H. Jee, J. Maiti and Y. S. Yoon, *Mater. Lett.*, 65 (2011) 3281.
13. Y. Li, W. Gao, L. Ci, C. Wang and P. M. Ajayan, *Carbon*, 48 (2010) 1124.
14. Y. Zhang, Y. Gu, S. Lin, J. Wei, Z. Wang, C. Wang, Y. Du and W. Ye, *Electrochim. Acta*, 56 (2011) 8746.
15. V. C. Tung, L. M. Chen, M. J. Allen, J. K. Wassei, K. Nelson, R. B. Kaner and Y. Yang, *Nano Lett.*, 9 (2009) 1949.
16. C. T. Hsieh, J. M. Wei, H. T. Hsiao and W. Y. Chen, *Electrochim. Acta*, 64 (2012) 177.
17. T. Maiyalagan, X. Dong, P. Chen and X. Wang, *J. Mater. Chem.*, 22 (2012) 5286.
18. S. Liu, J. Wang, J. Zeng, J. Ou, Z. Li, X. Liu and S. Yang, *J. Power Sources*, 195 (2010) 4628.
19. L. Wang, H. Zhu, H. Hou, Z. Zhang, X. Xiao and Y. Song, *J. Solid State Electrochem.*, 16 (2012) 1693.
20. J. Luo, S. Jiang, H. Zhang, J. Jiang and X. Liu, *Anal. Chim. Acta*, 709 (2012) 47.
21. L. Chen, Y. Tang, K. Wang, C. Liu and S. Luo, *Electrochem. Commun.*, 13 (2011) 133.
22. C. Gu and J. Tu, *Langmuir*, 27 (2011) 10132.
23. S. Park, J. An, R. D. Piner, I. Jung, D. Yang, A. Velamakanni, S. T. Nguyen and R. S. Ruoff, *Chem. Mater.*, 20 (2008) 6592.
24. Z. H. Ni, T. Yu, Y. H. Lu, Y. Y. Wang, Y. P. Feng, and Z. X. Shen, *ACS Nano*, 2 (2008) 2301.
25. K. Liu, J. Wei and C. Wang, *Electrochim. Acta*, 56 (2011) 5189.
26. A. C. Ferrari, J. Meyer, V. Scardaci, C. Casiraghi, M. Lazzeri, F. Mauri, S. Piscanec, D. Jiang, K. S. Novoselov, S. Roth and A. K. Geim, *Phys. Rev. Lett.*, 97 (2006) 187401.
27. H. Kang, A. Kulkarni, S. Stankovich, R. S. Ruoff and S. Baik, *Carbon*, 47 (2009) 1520.
28. D. Yang, A. Velamakanni, G. Bozoklu, S. Park, M. Stoller, R. D. Piner, S. Stankovich, I. Jung, D. A. Field, C. A. Ventrice and R. S. Ruoff, *Carbon*, 47 (2009) 145.
29. E. Casero, A. M. Parra-Alfambra, M. D. Petit-Domínguez, F. Pariente, E. Lorenzo and C. Alonso, *Electrochem. Commun.*, 20 (2012) 63.
30. M. Palomar-Pardavé, B. R. Scharifker, E. M. Arce and M. Romero-Romo, *Electrochim. Acta*, 50 (2005) 4736.
31. A. C. Hill, R. E. Patterson, J. P. Sefton and M. R. Columbia, *Langmuir*, 15 (1999) 4005.
32. W. Ye, D. Wang, H. Zhang, F. Zhou and W. Liu, *Electrochim. Acta*, 55 (2010) 2004.
33. A. J. Bard and L. R. Faulkner, *Electrochemical methods: Fundamentals and applications*, second ed. John Wiley and Sons Inc. New York, 2001.
34. P. V. Dudin, P. R. Unwin and J. V. Macpherson, *J. Phys. Chem. C*, 114 (2010) 13241.
35. V. G. Praig, G. Piret, M. Manesse, X. Castel, R. Boukherroub and S. Szunerits, *Electrochim. Acta*, 53 (2008) 7838.
36. B. Scharifker, and G. Hills, *Electrochim. Acta*, 28 (1983) 879.
37. Q. Shi and S. Mu, *J. Power Sources*, 203 (2012) 48.
38. C. Zhong, W. B. Hu and Y. F. Cheng, *J. Power Sources*, 196 (2011) 8064.
39. W. Ye, J. Liu, Q. Liu, F. Zhou and W. Liu, *Electrochim. Acta*, 55 (2010) 8649.
40. S. Sun, D. Yang, D. Villers, G. Zhang, E. Sacher and J. P. Dodelet, *Adv. Mater.*, 20 (2008) 571.
41. Y. Lin, X. Cui, H. C. Yen and C. M. Wai, *Langmuir*, 21 (2005) 11474.
42. G. Zhao, C. Xu, D. Guo and H. Li, *J. Power Sources*, 162 (2006) 492.
43. E. Yoo, T. Okata, T. Akita, M. Kohyama, J. Nakamura and I. Honma, *Nano Lett.*, 9 (2009) 2255.
44. Y. Hu, J. Jin, P. Wu, H. Zhang and C. Cai, *Electrochim. Acta*, 56 (2010) 491.

45. T. D. Jarvi, S. Sriramulu and E. M. Stuve, *J. Phys. Chem. B*, 101 (1997) 3649.  
J. Clavilier and D. Armand, *J. Electroanal. Chem.*, 199 (1986) 187.
46. K. Honda, M. Yoshimura, T. N. Rao, D. A. Tryk, A. Fujishima, K. Yasui, Y. Sakamoto, K. Nishio and H. Masuda, *J. Electroanal. Chem.*, 514 (2001) 35.
47. D. Guo and H. Li, *J. Power Sources*, 160 (2006) 44.